Baseline measurements in the assessment of ESS-specific radionuclide uptake by crops cultivated in Southern Sweden

Frost, Robert J. W.; Hermansson, Emma; Nagy, Gyula; Pédehontaa-Hiaa, Guillaume; Pongrac, Paula; Rääf, Christopher; Bernhardsson, Christian

LUND UNIVERSITY

PO Box 117
221 00 Lund
+46 46-222 00 00
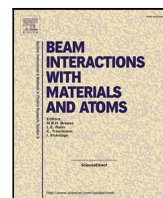
Baseline measurements in the assessment of ESS-specific radionuclide uptake by crops cultivated in Southern Sweden

R.J.W. Frost [a],*, E. Hermansson [a], G. Nagy [a], G. Pédehontaa-Hiaa [b], P. Pongrac [c,d], C.L. Rääf [b], C. Bernhardsson [b]

[a] Department of Physics and Astronomy, Uppsala University, Uppsala, Sweden
[b] Medical Radiation Physics Malmö, Lund University, Malmö, Sweden
[c] Biotechnical Faculty, University of Ljubljana, Ljubljana, Slovenia
[d] Department of Low and Medium Energy Physics, Joˇef Stefan Institute, Ljubljana, Slovenia

ABSTRACT

The European Spallation Source, ESS, is a neutron research facility under construction in Lund, Southern Sweden. The Facility will produce neutrons by spallation, using a powerful linear accelerator to deliver protons to a tungsten target. In addition to the desired neutron production, a long list of radionuclides will be created as by-products of the nuclear reaction inside the target. The Swedish Radiation Safety Authority has established a list of the most relevant radionuclides, in terms of contribution to the effective dose to ESS workers and the general public, should an accidental release of irradiated target material occur. This list includes radionuclides that are not produced by the nuclear energy industry, in particular ^{178m}Hf, ^{182}Ta, ^{187}W, ^{148}Gd and ^{173}Lu. Ongoing research efforts aim to determine the best analytical methods to assess these exotic and often difficult-to-measure radionuclides in environmental samples. This work investigates the potential of X-ray fluorescence and time-of-flight elastic Recoil detection analysis for the assessment of soil samples, and the potential of particle induced X-ray emission for the assessment of crop samples. These techniques require only simple sample preparation steps and no chemical extraction, unlike the conventional environmental monitoring methods such as inductively-coupled plasma mass spectrometry, and show promise as complimentary methods enabling fast sample throughput. This study focuses on the analysis of uncontaminated soil and crops, to provide baseline data, whilst simultaneously assessing the available measurement capabilities. For the X-ray fluorescence system used in this study, the method detection limit for W in soil was determined to be 0.147 ppth, and Zr which can be correlated with the migration of Hf was clearly measurable.

1. Introduction

The ESS (European Spallation Source) [1,2] is a large neutron research facility under construction outside of Lund, Sweden. The ESS will produce neutrons through spallation, by delivering a pulsed 2 GeV proton beam with an average power of 5 MW to a 3000 kg tungsten target. In addition to neutrons, the spallation process in the target will also produce a long list of radioactive by-products. Due to the uniqueness of the beam-energy-target combination employed, the radionuclides in question are very specific to the ESS, and many do not appear as a result of activities at more conventional nuclear facilities, or elsewhere in society. An understanding of how these radionuclides will behave in the environment is therefore necessary in the event, however unlikely, that they are released into the environment through a severe accident [3].

The ESS target will be regularly replaced, every five years, and simulations predicting the radionuclide inventory during and after operational life of each target have been performed [5]. As operation of the ESS has not yet started however, no verification of these simulations is yet available, as it is for similar facilities [6], and small deviations from the predicted inventories cannot be ruled out. Assessment of environmental consequences of the normal operations of the ESS facility have been reported in detail [7] including, for example, activation assessments of the soil around the ESS accelerator tunnel [8]. In 2018, a dimensional accidental scenario of the ESS facility was described by SSM (the Swedish Radiation Safety Authority) [4] showcasing a list of the radionuclides, presented in Table 1, that would contribute most to the effective dose received by a representative person from exposure to ground deposition, following a worst-case accident. According to this accident scenario, the radioactive material of the ESS target would be emitted as an aerosol. Either wet or dry ground deposition would then

Table 1

Radionuclides that, in the worst-case accident scenario [4], are predicted to form the primary contribution to the effective dose from ground deposition during the first year after release.

Nuclide	$T_{1/2}$	Decay mode	Daughter	Daughter $T_{1/2}$	Daughter decay mode	Granddaughter
^{148}Gd	74.6 y	Pure α	^{144}Sm	Stable		
^{187}W	24 h	β, γ	^{187}Re	4E+10 y	Pure β	^{187}Os (stable)
^{172}Hf	1.87 y	EC, γ	^{172}Lu	6.7 d	$β^+$, γ	^{172}Yb (stable)
^{182}Ta	111.7 d	β, γ	^{82}W	Stable		
^{178m}Hf	31 y	IT	^{178}Hf	Stable		
^{181}W	121.2 d	EC	^{181}W	Stable		
^{175}Hf	70 d	EC	^{175}Lu	Stable		
^{173}Lu	1.37 y	EC	^{173}Y	Stable		

occur, depending on the weather conditions, following which spallation products would start to migrate through the soil column. The uptake of the deposited spallation products by plants would occur either through the root system, from direct interception into the leaf/crop matrix, or a combination of both. The fraction attributed to root uptake in a given species will depend on the local soil conditions and seasonality. This scenario, currently forms the basis for dimensioning the emergency preparedness zones and site category classification according to IAEA 2015 guidelines [9]. The fact remains however, that the migration of the elements listed in Table 1, in soil, has rarely been studied and experimental data on the accumulation of these metals in plants is scarce [10]. Data on the transfer of these metals in the environment is lacking in the IAEA reference handbook [11] and, consequently, large uncertainties exist regarding their fate if released into the environment [12].

Environmental contamination by stable W, Hf and Ta usually originate from industrial- [13], military- [14] and agricultural-activities [15], as well as from road traffic [16]. Unlike Gd, for which concentrations exceeding 200 μmol/l in the substrate were shown to be toxic to Arabidopsis thaliana [17], W, Hf and Ta are not considered to be toxic and the behaviour of these elements in the environment is not well studied. W has, however, drawn more attention in the recent years due to a possible connection to cases of leukaemia in the United States [14], and one study from China on the binding and association of W with different soil components [13] has found that soil organic matter retained tungsten in soils deeper than 70 cm. The information available on environmental Ta is summarised in only one review by Filella [18], and most of the literature found on Hf in the environment is linked to its separation from Zr. Knowledge on the transfer of the elements from soil to plants grown on the lands surrounding the ESS is also very limited, with only one study on the transfer of Hf and Ta to barley [19] and two on the transfer/toxicity of W to corn and peas [20,21]. The lack of available transfer parameters for the ESS-related metals between environmental compartments (i.e. soil, water, plants) currently prevents the development of region-specific radioecological models [12]. Obtaining such parameters from experimental data is essential, and recent work to improve the external-dose estimates following an accidental radiological release from ESS [22], shows that wide variation in the long-term external dose results from parameter adjustment. Investigation of the limits-of-detection for ESS-specific radionuclides in soil has been performed by Inductively Coupled Plasma Mass Spectrometry (ICP-MS) [10,12], and investigations have even been made into the possibility of using cyclic neutron-activation analysis [23] with future compact accelerator-driven neutron sources [24,25]. The ICP-MS investigations did not indicate any current contamination of the site by the metals of interest, but the resistance of some of these metals to chemical extraction highlighted the limits of ICP-MS. There is indeed a need for other analytical techniques that would not require heavy sample preparation, in particular in the case of emergency situations.

In the present work, a preliminary investigation is made into the applicability of IBA (ion-beam analysis) techniques, to investigate metal concentrations in the environment, through measurements on samples obtained as part of the "zero-point" radiological assessment [26] of the lands surrounding the ESS site. It is not the intention that these techniques will replace the use of mass spectroscopy techniques, but to use

them complimentary analysis options to increase sample throughput. The samples analysed in this work are free from the contaminants that are of interest to the broader study, and therefore represent important baseline data to support further studies.

2. Methodology

Soil samples studied in this work were collected from the sites around the ESS facility shown in Fig. 1(a), with GPS coordinates given in Table 2, as part of the "zero-point" project [26] and the ongoing environmental monitoring program performed by Lund University. Crop samples studied in this work, were collected from harvests, grown in the fields indicated in Fig. 1(b). All sample measurements in this project were carried out at the Tandem Laboratory, Uppsala University [27]. In total, five soil samples and three crop samples were analysed, these representing baseline measurements on uncontaminated samples.

The soil samples were pressed into pellets, 15.5 mm in diameter, and placed in a ventilated oven at 50 °C for 24 h to remove moisture content. The pellets were then weighed, and the thickness of each was measured to determine density. ToF-ERDA (Time-of-Flight Elastic Recoil Detection Analysis) measurements were carried out on each pellet using a 36 MeV ^{79}Br^{8+} primary-ion beam, at an incidence angle of 67.5° to the sample normal, and recoiled ions detected at an angle of 45° to the primary beam. The measured ToF-ERDA spectra were converted into depth-dependent relative atomic concentration profiles using the Potku software package [28]. XRF (X-ray Fluorescence) measurements on each pellet were performed using a table-top setup consisting of an Amptek Mini-X X-ray tube, with Ag anode and an Amptek X-123SDD silicon drift detector with an active thickness of 5 mm and a 12.5 μm Be window. The X-ray tube was operated at 40 kV and 50 μA, using a measurement time of 1800 s for all samples. All measurements were performed in air, with source-to-sample and sample-to-detector distances both set at 3 cm. During measurement, samples were supported on a 13 μm Mylar film, with a 3 mm thick Al-plate shielding the detector from X-rays that could be scattered from chamber components after passing through the sample. The recorded X-ray spectra were analysed using the PyMCA software package [29], in which the flux of the X-ray source was calibrated using measurements on a stoichiometric TiVZrNbHf alloy. Certified standards NCS-DC73323a (industrial soil, LGC Standards, certificate expiry Aug-2021) and BRC-667 (estuarine sediment, JRC, certificate expiry Dec-2029) were then analysed to assess the reliability of elemental quantification, and determine systematic uncertainties for the system used. The sample-matrix composition used to define self-attenuation in the XRF analysis, was derived from the ToF-ERDA measurement results. For this derivation, the elements in the soil samples were assumed to be found as oxides and the oxygen content, given by the ToF-ERDA analysis, was thus divided between the other elements according to their atomic fraction and most naturally abundant oxide form. The molecular percentages of these oxides were then converted to molecular mass-fractions for entry into PyMCA.

To assess the method detection limit of W in the soil samples studied, additional pellets of one soil sample (E3) were produced with different concentrations of W added to each pellet prior to pressing. W

Table 2
GPS coordinates, for the sampling locations, for each of the soil samples analysed in the present work.

Sample	Location	
E3	N55.74310	E13.24773
E52	N55.73472	E13.24184
E258	N55.7284	E13.25561
E331	N55.73343	E13.25866
E344	N55.73796	E13.27053

was added in the form of WC, in concentrations of 1%, 0.5%, and 0.1% by weight. XRF analysis was then performed on each pellet according to the same procedure used for the other soil samples.

Seed samples were cut into 1 mm thick sections and mounted on an adhesive carbon-based backing for μ-PIXE (Particle induced X-ray Emission) analysis. The μ-PIXE analysis was carried out at the scanning light-ion microprobe [30] in Uppsala, using a 2.5 MeV proton beam with an average current of around 100 pA and a spot size of approximately 5 μm, scanned over an area of 1×1 mm^2. Measurement time for each sample was between 2.5 and 3.5 h. The X-ray detector used was a Princeton Gamma-Tech Si(Li), with an active thickness of 5 mm and a Be window with a thickness of 12.5 μm, positioned at a distance of 2.5 cm from the sample at an angle of 135° to the incident proton beam. Analysis of the PIXE spectra was performed using GeoPIXE [31,32], to produce elemental-concentration maps of each sample as well as extracting the total elemental concentrations.

3. Results and discussion

3.1. Analysis of soil using combined XRF and ToF-ERDA

Elemental concentrations, determined by XRF analysis, for reference samples NCS-DC73323a and BRC-667 are presented in Tables 3 and 4 respectively. Uncertainties include the statistical fitting uncertainty obtained individually for each element from PyMca, as well as a fixed 22% systematic uncertainty for all elements. Empty entries in Table 4 are due to no certified value being given. Measured values agree with certified values within the uncertainties. Elemental concentrations measured using ToF-ERDA and XRF, for each soil sample, are shown in Tables 5 and 6 respectively, where empty entries indicate that no clear signals above background were observable. With regards to the XRF results, elements with proton numbers lower than that of K were not measurable due to absorption in the detector window and interference from the Ar K-lines. Measured concentrations were cross-checked against those listed in the Geochemical Atlas of Europe [33]. For those elements presented in Table 6, reasonable agreement was found in most cases: measured concentrations for Ca, Ti, Mn and Fe were found to be generally lower than documented for the area, while measured values for Cu, Zn and Rb were higher by a factor of two in all samples. Values for Sr and Zr fall within the expected range for all samples. A number of lanthanides were identified in the XRF spectra of some samples which matched well with the typical values given in the Geochemical Atlas of Europe; Tb, Dy, Ho, Er, Tm, Yb, and Lu were identified in sample E52 for example, but as the uncertainties on these measurements put them far outside of the method detection limits, they have been excluded from Table 6.

For all cases in Table 5, concentrations were obtained by integrating the elemental depth-profiles, given by Potku, over a depth range of 500 to 1000×10^{15} atoms/cm^2. The detection limit of around 0.5 atomic % is typical for the setup used, although it can be seen that statistical uncertainties become large as this limit is approached. Within this limit-of-detection, ToF-ERDA is sensitive to the entire periodic table, with the exception being to elements with masses close to that of the primary-ion beam used as signals from these elements are masked by signals from the primary beam being scattered into the detector.
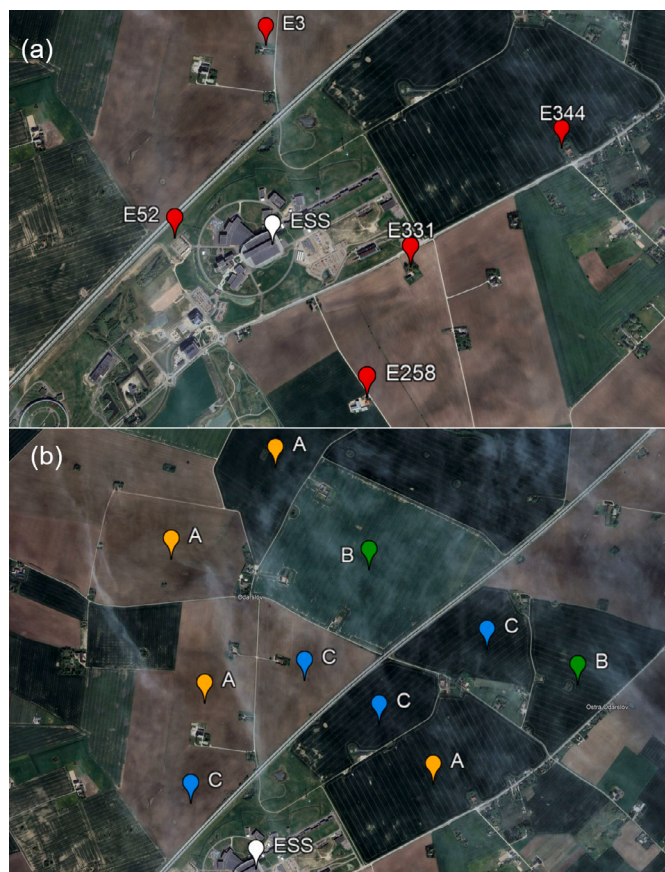

Fig. 1. Maps of the north-eastern part of Lund from were samples were taken: (a) indicates sites for soil sampling, and where measurements of ambient dose rate and in situ gamma spectroscopy were also performed; (b) indicates locations of the fields where crops A -rapeseed, B - barley and C - wheat were sampled.
Source: Figure adapted from [10,26].

A second caveat of the ToF-ERDA results, is that they are unable to separate elements very close in mass, at least for masses greater then Ne. Examples of this inseparability, seen in Table 5, are Al-Si, K-Ca and Mn-Fe, for which a combined atomic % is given. Intercomparison between the data in Tables 5 and 6 can only be made in terms of Ti, Mn and Fe, for which inconsistencies are observed. It should be noted here that only statistical uncertainties are accounted for in the ToF-ERDA results. In the case of Ti, the concentrations are very close to the detection limit, and the influence of background counts can easily account for the discrepancies observed. For Fe and Mn, the mixing of other elements close in mass cannot be ruled out. These particular cases, however, are not considered to be of great issue in the context of these measurements, as the purpose of the ToF-ERDA data is to provide information on the lighter elements that make up the bulk of each sample and thus provide an estimate of the sample matrix for the XRF analysis. The purpose has clearly been fulfilled, as demonstrated by the data presented in Tables 3 and 4.

Combined, the data presented in Tables 5 and 6 shows promise for the use of combined IBA techniques in the analysis of such environmental samples. Elements in the range from H to Pb are covered by the data, with the only gap being Al-Si, which is missed by the XRF data due to poor low-energy detector-efficiency and only presented as a combined value in the ToF-ERDA results. It should also be noted that, other than pellet pressing and very basic dehydration, no sample preparation was necessary to obtain the data presented. With relatively

Table 3
Elemental concentrations for reference sample NCS-DC73323a, both certified and as determined through XRF analysis in the present work.

Element	Concentration [mass ppth]	
	Certified	Measured
K	17.76 ± 0.50	17.46 ± 4.13
Ti	6.10 ± 0.30	6.10 ± 1.41
Mn	0.51 ± 0.02	0.47 ± 0.14
Fe	70.08 ± 1.47	69.20 ± 15.33
Cu	0.15 ± 0.01	0.18 ± 0.05
Zn	0.17 ± 0.01	0.23 ± 0.06
As	0.24 ± 0.02	0.31 ± 0.08
Rb	0.14 ± 0.01	0.23 ± 0.06
Sr	0.04 ± 0.00	0.07 ± 0.02
Zr	0.27 ± 0.01	0.37 ± 0.09
Pb	0.25 ± 0.01	0.39 ± 0.10

Table 4
Elemental concentrations for reference sample BRC-667, both certified and as determined through XRF analysis in the present work.

Element	Concentration [mass ppth]	
	Certified	Measured
Cl		38.78 ± 9.78
K		22.59 ± 5.27
Ca		45.06 ± 10.16
Ti		3.46 ± 0.83
Cr	0.18 ± 0.02	0.31 ± 0.10
Mn	0.92 ± 0.04	0.71 ± 0.20
Fe	44.80 ± 1.00	46.65 ± 10.35
Ni	0.13 ± 0.01	0.05 ± 0.02
Cu	0.06 ± 0.01	0.09 ± 0.03
Zn	0.18 ± 0.01	0.24 ± 0.06
As	0.02 ± 0.00	0.05 ± 0.02
Br	0.10 ± 0.00	0.12 ± 0.03
Rb		0.19 ± 0.05
Sr	0.22 ± 0.02	0.32 ± 0.08
Zr		0.15 ± 0.04

minor adjustment of the measurement setup, this methodology has the potential to provide an effective and high through-put solution to soil analysis.

3.2. Determining detection limits of W in soil

The separability of elemental signals in XRF, although greatly better than for ToF-ERDA at the higher end of the periodic table, is not an issue that can be completely ignored in complex samples such as soils. Detection limits also reduce for XRF as proton number increases, due to reducing X-ray production cross sections, limited primary X-ray energy and, in the present case, reduced detector efficiency in the high energy region. The soil samples, for which results are presented in Section 3.1, are uncontaminated and significant amounts of Gd, Hf, Ta and W are not anticipated. It is important, however, to determine the detection limits of elements such as Gd, Hf, Ta and W in such samples, as they will be of primary interest in future studies in which doped samples will be analysed.

Fig. 2(a) shows the normalised XRF spectra recorded for the E3 sample pellet, as well as the E3 pellets with added WC. The positions of the W L-lines are marked in Fig. 2(a), and the positions of peaks from Cu and Zn are also labelled. It is clear from these data that any spectrum from a sample, such as soil, which contains all four of these elements will be challenging to deconvolve, and detection limits for these elements will be compromised to some degree. Fig. 2(b) shows the mass fractions, extracted from the spectra in Fig. 2(a), as a function of the W concentration in the sample. Uncertainties on the W concentrations are estimated at 0.5 ppth of the total sample mass, based on the ability to accurately weigh the small quantities of WC required for mixing with each pellet. The same uncertainty has been assigned to

the 0% W sample, as a complete absence of W cannot be truly ruled out. Uncertainties on the measured mass fractions of W are assigned in the manner described in Section 3.1. The shaded region in Fig. 2(b) shows the 95% confidence interval on the fit to the data points. The method detection limit for W is taken to be the point at which the 95% confidence interval meets the X-axis, this being 0.147 ppth.

Although a detection limit for Hf is not explicitly investigated here, it is interesting to highlight that Zr is observed in all samples. As Zr and Hf present almost identical chemical behaviour [34], it is possible to infer the behaviour of Hf that is artificially introduced into an environment system, based on the behaviour of Zr [35].

3.3. Analysis of crop samples using μ-PIXE

Fig. 3 and Table 7 show selected elemental-maps and total elemental-concentrations, respectively, of the three crop samples analysed by μ-PIXE. The elemental maps presented in Fig. 3, show varying distributions of Ca, K, Fe and Zn, with Ca seen to be primarily located in the husks of the seeds while P, K, Fe and Zn are concentrated in the aleurone layer responsible for the immobilisation of essential elements bound to phytic acid [36]. Concentration of these elements in outer layers of the seeds is commonly observed and often used as the basis for promoting whole grains in diet [37] but, in this context, also implies that food products made from seeds with the husk removed will be less likely to carry contamination into the food chain. The wider range of elements shown in Table 7, demonstrates that elements up to Cd can be detected in such samples, with concentrations as low as 0.5 ppm, although no Ta, Hf or W was observed above background in these measurements. Much like the XRF analysis described above, the PIXE measurements are somewhat limited for higher proton-number elements by low-detection efficiencies for higher X-ray energies, which will be addressed in the future by exchange of the detector system. Unlike the XRF analysis however, for which the energy of the primary X-rays is limited by the X-ray source, much higher proton energies can be used for future PIXE analysis increasing the X-ray production cross-sections for the heavier elements. This increase in proton energy comes at the cost of a thicker window on the X-ray detector, to shield it from back-scattered protons, but as it is higher-energy X-rays from heavier elements that are of interest the loss in efficiency for lower-energy X-rays can be tolerated.

Another area for improvement in the PIXE measurements, is that there was no independent verification of the sample matrix as was performed for the XRF measurements. In the present work, a generic H-C-N-O matrix for biological material was assumed and entered into GeoPIXE. This assumed matrix composition has potential to skew absolute concentrations calculated by GeoPIXE, due to the potential for incorrectly calculated self-attenuation; the results presented in Table 7 should thus be considered as semi-quantitative only. One solution to the matrix-composition issue is to perform simultaneous OA-STIM (Off Axis - Scanning Transmission Ion Microscopy) and μ-PIXE [38–41]. In such a measurement, OA-STIM will constrain the H-C-N-O ratios in samples on a pixel-by-pixel basis; these elements constituting the majority of the sample matrix. To implement OA-STIM, samples will be sectioned to a thickness of ∼20 μm and pioloform films used to suspend the samples while still allowing for ion transmission. The procedure for this will be refined and implemented in the near future.

4. Summary and outlook

Based on the existing source term calculations for the composition of the ESS tungsten target, the Swedish Radiation Safety Authority has established a list of radionuclides of most concern in case of environmental release including [178m]Hf, [182]Ta, [187]W, [148]Gd and [173]Lu. In this work, the potential of applying IBA techniques and XRF to analyse soil and crop samples for evidence of these elements has been investigated, through the study of uncontaminated environmental samples. This

Table 5

Elemental concentrations, determined through ToF-ERDA analysis, for five different soil samples (denoted E331, E344, E52, E258 and E3, respectively) collect from the lands surrounding the ESS. Data analysis was performed in Potku [28] to obtain concentrations in atomic %, which were then converted to mass ppth. The uncertainties quoted are derived only from counting statistics in the measured ToF-ERDA spectra for each element.

Element	Concentration [mass ppth]				
	E331	E344	E52	E258	E3
H	1.7 ± 0.5	1.5 ± 0.6	0.8 ± 0.0	0.0 ± 0.0	0.1 ± 0.0
C	18.4 ± 1.2	27.7 ± 1.8	16.2 ± 2.3	8.4 ± 1.7	15.0 ± 1.2
N	4.6 ± 0.7	5.2 ± 0.8	4.7 ± 1.3	3.3 ± 1.3	6.5 ± 0.9
O	483.6 ± 7.1	469.5 ± 7.9	468.8 ± 7.7	446.5 ± 14.9	483.6 ± 8.4
Mg	13.6 ± 1.3	20.3 ± 2.4	17.5 ± 3.5	18.1 ± 4.5	19.8 ± 2.3
Al & Si	403.6 ± 6.9	382.4 ± 8.3	392.6 ± 14.8	380.2 ± 18.3	352.5 ± 8.1
P			4.2 ± 1.9	0.0 ± 0.0	2.3 ± 0.8
K & Ca	33.6 ± 2.4	45.3 ± 0.4	44.3 ± 5.8	67.1 ± 9.3	51.8 ± 3.8
Ti			5.3 ± 1.8	8.9 ± 4.5	8.9 ± 1.6
Mn & Fe	38.9 ± 2.8	48.0 ± 3.6	45.6 ± 5.4	67.5 ± 10.4	58.9 ± 5.4

Table 6

Elemental concentrations, determined through XRF analysis, for five different soil samples collected from the lands surrounding the ESS. Data analysis was performed using PyMCA [29]. Uncertainties quoted include both peak-fitting uncertainties given by PyMCA, and a fixed systematic uncertainty.

| Element	Concentration [mass ppth]				
	E331	E344	E52	E258	E3
K	22.61 ± 5.24	16.06 ± 3.77	22.86 ± 5.31	25.68 ± 5.94	27.40 ± 6.32
Ca	7.10 ± 1.69	6.37 ± 1.52	5.78 ± 1.40	7.66 ± 1.83	7.86 ± 1.87
Ti	3.43 ± 0.82	2.20 ± 0.54	3.55 ± 0.84	4.37 ± 1.03	4.02 ± 0.95
Mn	0.61 ± 0.17	0.29 ± 0.09	0.27 ± 0.09	0.28 ± 0.09	0.55 ± 0.15
Fe	23.75 ± 5.29	19.42 ± 4.34	29.22 ± 6.50	28.30 ± 6.29	26.72 ± 5.94
Ni	0.05 ± 0.02	0.03 ± 0.02			
Cu	0.01 ± 0.01	0.03 ± 0.02	0.10 ± 0.03	0.04 ± 0.02	0.05 ± 0.02
Zn	0.58 ± 0.14	0.15 ± 0.04	0.20 ± 0.05	0.25 ± 0.06	0.24 ± 0.06
As	0.07 ± 0.02	0.05 ± 0.02		0.04 ± 0.02	
Rb	0.18 ± 0.05	0.14 ± 0.04	0.20 ± 0.05	0.17 ± 0.04	0.19 ± 0.05
Sr	0.19 ± 0.05	0.14 ± 0.04	0.19 ± 0.05	0.21 ± 0.05	0.16 ± 0.04
Zr	0.52 ± 0.12	0.31 ± 0.07	0.38 ± 0.09	0.42 ± 0.10	0.43 ± 0.10
Pb				0.13 ± 0.04	
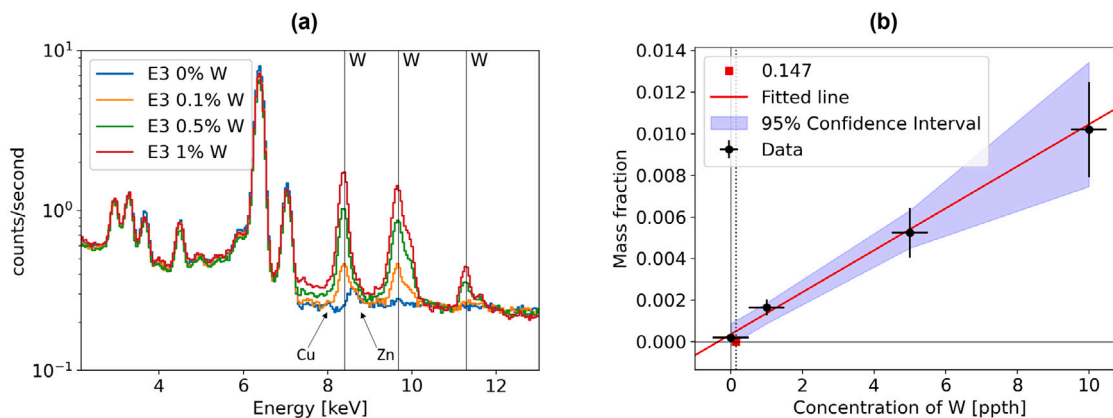
Fig. 2. Determination of XRF method detection limit for W in soil: (a) XRF spectra for soil samples doped with varying quantities of WC.; (b) fitted W concentration data, with the 95% confidence interval giving the method detection limit by its zero-crossing.

study is part of an onging effort to determine the best methodologies for measuring environmental transfer parameters, that will enable accurate modelling of the migration of these nuclei in the environment, and thus advise emergency-preparedness protocols relating to the ESS.

Five soil samples, collected from around the ESS facility, were analysed by combined ToF-ERDA and XRF, and three crop samples were analysed by μ-PIXE. The benefit of combining ToF-ERDA and XRF is clearly demonstrated, with ToF-ERDA providing concentrations of the more abundant light-elements and thus providing a well-categorised sample matrix for the XRF analysis. A method detection limit for W was determined to be 0.147 ppth, for a representative soil sample. Zr was also found to be measurable in all soil samples and can be used to

infer the behaviour of Hf, even if Hf concentrations are below detection limits.

The elemental-concentration maps generated from analysis of the μ-PIXE data, show elemental distributions that correlate with expectations based on the literature. In future, higher proton-energies will be used, an X-ray detector with greater efficiency in the high-energy region implemented and samples prepared in a way that will allow for OA-STIM to be performed in the same measurement. Nevertheless, it has been showed that the proper combination of IBA methods seems a promising way to qualitatively assess potential soil contaminations and their entry into the food-chain through crops.

Further studies are planned for the near future, in which soil artificially doped with W, Hf and Ta will be analysed after different
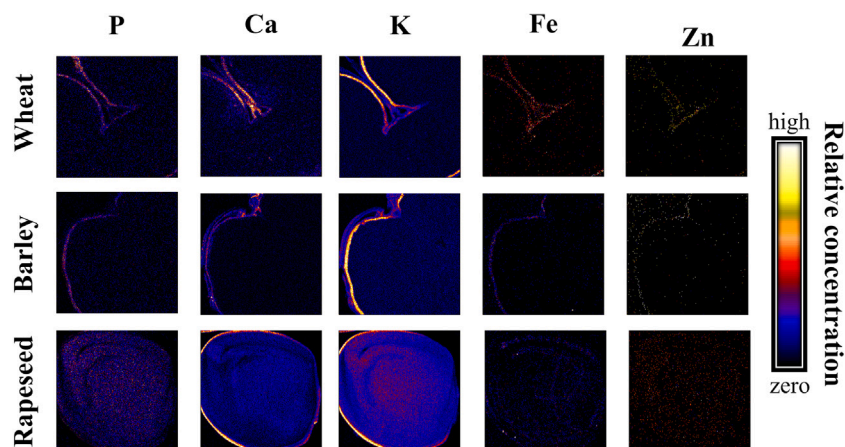
Fig. 3. Elemental-concentration maps, for three different seed types, derived from μ-PIXE analysis. Measurements were performed using the nuclear μ-probe at Tandem Laboratory [30], and data analysis was performed using GeoPIXE. Each map is 256×256 pixels, and covers an area of $1 \times 1\,\text{mm}^2$.

Table 7
Elemental concentrations, determined through μ-PIXE analysis, for three different seed types. Measurements were performed using the nuclear μ-probe at Tandem Laboratory [30], and data analysis was performed using GeoPIXE. All concentrations are expressed in ppm.

Element	Concentration [mass ppm]		
	Wheat	Barley	Rapeseed
P	4546 ± 344	4140 ± 310	$16\,687 \pm 765$
S	1811 ± 129	1523 ± 103	6270 ± 97
Cl	1487 ± 28	752 ± 25	561 ± 30
K	2131 ± 20	1218 ± 13	4715 ± 24
Ca	247 ± 8	143 ± 7	1313 ± 14
Mn	3.9 ± 0.5	1.4 ± 0.3	12 ± 1
Fe	16 ± 0.5	7.4 ± 0.8	33 ± 1
Cu	1.2 ± 0.5	1.3 ± 0.4	2.6 ± 0.4
Zn	5.5 ± 0.9	5.5 ± 0.5	26 ± 3
Br	4 ± 1	$<1.6 \pm 0.7$	$<1.4 \pm 0.6$

weathering periods to assess elemental migration. Cultivation of crops in doped soil will also be performed, and crop samples analysed to assess dopant uptake. Results will be used to support future modelling of the dispersion of the ESS-related radioisotopes in the environment. This continued work will forward knowledge in the field of radiation protection, and advise future emergency-preparedness measures for the general public.

Declaration of competing interest

The authors declare that they have no known competing financial interests or personal relationships that could have appeared to influence the work reported in this paper.

Acknowledgements

References

[1] R. Garoby, A. Vergara, H. Danared, I. Alonso, E. Bargallo, B. Cheymol, C. Darve, M. Eshraqi, H. Hassanzadegan, A. Jansson, I. Kittelmann, Y. Levinsen, M. Lindroos, C. Martins, O. Midttun, R. Miyamoto, S. Molloy, D. Phan, A. Ponton, E. Sargsyan, T. Shea, A. Sunesson, L. Tchelidze, C. Thomas, M. Jensen, W. Hees, P. Arnold, M. Juni-Ferreira, F. Jensen, A. Lundmark, D. McGinnis, N. Gazis, J.W. II, M. Anthony, E. Pitcher, L. Coney, M. Gohran, J. Haines, R. Linander, D. Lyngh, U. Oden, H. Carling, R. Andersson, S. Birch, J. Cereijo, T. Friedrich, T. Korhonen, E. Laface, M. Mansouri-Sharifabad, A. Monera-Martinez, A. Nordt, D. Paulic, D. Piso, S. Regnell, M. Zaera-Sanz, M. Aberg, K. Breimer, K. Batkov, Y. Lee, L. Zanini, M. Kickulies, Y. Bessler, J. Ringnér, J. Jurns, A. Sadeghzadeh, P. Nilsson, M. Olsson, J.-E. Presteng, H. Carlsson, A. Polato, J. Harborn, K. Sjögreen, G. Muhrer, F. Sordo, The European spallation source design, Phys. Scr. 93 (1) (2017) 014001, http://dx.doi.org/10.1088/1402-4896/aa9bff.

[2] S. Peggs, ESS Technical Design Report, Tech. Rep. ESS-DOC-274, ESS, 2013.

[3] K.E. Stenström, V. Barkauskas, G. Pédehontaa-Hiaa, C. Nilsson, C. Rääf, H. Holstein, S. Mattsson, J. Martinsson, M. Jönsson, C. Bernhardsson, Identifying Radiologically Important ESS-Specific Radionuclides and Relevant Detection Methods, Tech. Rep. 2020:08, SSM, 2020.

[4] A.M. Blixt Buhr, J. Johansson, P. Kock, J. Boson, S. Karlsson, J. Lindgren, E. Tengborn, ESS research facility: Basis for emergency preparedness and response planning, Tech. Rep. 2018:22e, SSM, 2018.

[5] V. Barkauskas, K. Stenström, Prediction of the radionuclide inventory in the European Spallation source target using FLUKA, Nucl. Instrum. Methods Phys. Res. B 471 (2020) 24–32, http://dx.doi.org/10.1016/j.nimb.2020.03.013.

[6] D.J.S. Findlay, G.P. Škoro, G.J. Burns, S. Ansell, Experimental verification of spallation inventory calculations, Appl. Radiat. Isot. 125 (2017) 1–3, http://dx.doi.org/10.1016/j.apradiso.2017.03.023.

[7] D. Ene, R. Avila, T. Hjerpe, D. Bugay, K. Stenberg, Assessment of environmental consequences of the normal operations of the ESS facility, J. Phys. Conf. Ser. 1046 (1) (2018) 012018, http://dx.doi.org/10.1088/1742-6596/1046/1/012018.

[8] I.L. Rakhno, N.V. Mokhov, I.S. Tropin, D. Ene, Activation assessment of the soil around the ESS accelerator tunnel, J. Phys. Conf. Ser. 1046 (1) (2018) 012020, http://dx.doi.org/10.1088/1742-6596/1046/1/012020.

[9] Preparedness and Response for a Nuclear or Radiological Emergency, in: General Safety Requirements, Vol. GSR Part 7, IAEA, Vienna, 2015, http://dx.doi.org/10.61092/iaea.3dbe-055p.

[10] G. Pédehontaa-Hiaa, R.J.W. Frost, V. Barkauskas, K.E. Stenström, M. Elfman, C. Bernhardsson, C. Rääf, Investigation of the Limits of Detection for Specific Radionuclides in Soil from the European Spallation Source (ESS) Using Radiometric and Mass Spectrometric Methods, Tech. Rep. 2023:12, SSM, 2023.

[11] Handbook of Parameter Values for the Prediction of Radionuclide Transfer in Terrestrial and Freshwater Environments, Tech. Rep. Technical Report Series no. 472, IAEA, 2010.

[12] G. Pédehontaa-Hiaa1, C. Bernhardsson, V. Barkauskas, K.E. Stenström, C. Rääf, S. Mattsson, Region-Specific Radioecological Evaluation of Accidental Releases of Radionuclides from ESS, Tech. Rep. 2021:21, SSM, 2021.

[13] H. Du, Y. Li, D. Wan, C. Sun, J. Sun, Tungsten distribution and vertical migration in soils near a typical abandoned tungsten smelter, J. Hazard. Mater. 429 (2022) 128292, http://dx.doi.org/10.1016/j.jhazmat.2022.128292.

[14] A. Koutsospyros, W. Braida, C. Christodoulatos, D. Dermatas, N. Strigul, A review of tungsten: From environmental obscurity to scrutiny, J. Hazard. Mater. 136 (1) (2006) 1–19, http://dx.doi.org/10.1016/j.jhazmat.2005.11.007.

[15] Y. Yang, Y. Wang, P. Westerhoff, K. Hristovski, V.L. Jin, M.-V.V. Johnson, J.G. Arnold, Metal and nanoparticle occurrence in biosolid-amended soils, Sci. Total Environ. 485–486 (2014) 441–449, http://dx.doi.org/10.1016/j.scitotenv.2014.03.122.

[16] M. Bäckström, U. Nilsson, K. Håkansson, B. Allard, S. Karlsson, Speciation of heavy metals in road runoff and roadside total deposition, Water Air Soil Pollut. 147 (1) (2003) 343–366, http://dx.doi.org/10.1023/A:1024545916834.

[17] Z. Liu, C. Guo, P. Tai, L. Sun, Z. Chen, The exposure of gadolinium at environmental relevant levels induced genotoxic effects in Arabidopsis thaliana (L.), Ecotoxicol. Environ. Saf. 215 (2021) 112138, http://dx.doi.org/10.1016/j.ecoenv.2021.112138.

[18] M. Filella, Tantalum in the environment, Earth-Sci. Rev. 173 (2017) 122–140, http://dx.doi.org/10.1016/j.earscirev.2017.07.002.

[19] I. Shtangeeva, Accumulation of scandium, cerium, europium, hafnium, and tantalum in oats and barley grown in soils that differ in their characteristics and level of contamination, Environ. Sci. Pollut. Res. 29 (27) (2022) 40839–40853, http://dx.doi.org/10.1007/s11356-021-18247-y.

[20] G. Petruzzelli, F. Pedron, Influence of increasing Tungsten concentrations and soil characteristics on plant uptake: Greenhouse experiments with Zea mays, Appl. Sci. 9 (19) (2019) http://dx.doi.org/10.3390/app9193998.

[21] I.-D.S. Adamakis, E.P. Eleftheriou, T.L. Rost, Effects of sodium tungstate on the ultrastructure and growth of pea (Pisum sativum) and cotton (Gossypium hirsutum) seedlings, Environ. Exp. Bot. 63 (1) (2008) 416–425, http://dx.doi.org/10.1016/j.envexpbot.2007.12.003.

[22] C. Raaf, R.J.W. Frost, C. Bernhardsson, G. Pédehontaa-Hiaa, External doses from an accidental release of ESS spallation-target products – Time-dependence and radionuclide contribution, under review for the Nordic Society of Radiation Protection conference proceedings. manuscript number: RPD-24-0105.

[23] R.J.W. Frost, M. Elfman, P. Kristiansson, J. Lindsey-Clark, C. Maurer, J. Pallon, G. Pédehontaa-Hiaa, The prototyping of a high-resolution neutron activation analysis system – based on a pelletron accelerator and fast pneumatic sample-transport, J. Phys. Conf. Ser. 2326 (1) (2022) 012019, http://dx.doi.org/10.1088/1742-6596/2326/1/012019.

[24] R.J.W. Frost, M. Elfman, K. Fissum, M. Kristensson, P. Kristiansson, N. Mauritzson, J. Pallon, H. Perrey, G. Pédehontaa-Hiaa, A. Sjöland, K. Stenström, Development of a Pelletron-based compact neutron source, J. Neutron Res. 24 (3–4) (2022) 281–287, http://dx.doi.org/10.3233/JNR-220026.

[25] R.J.W. Frost, M. Elfman, K. Fissum, P. Kristiansson, N. Mauritzson, J. Pallon, G. Pédehontaa-Hiaa, H. Perrey, K.E. Stenström, A. Sjöland, A compact accelerator driven neutron source at the Applied Nuclear Physics Laboratory, Lund University, EPJ Tech. Instrum. 10 (1) (2023) 14, http://dx.doi.org/10.1140/epjti/s40485-023-00101-9.

[26] C. Bernhardsson, K.E. Stenström, M. Jönsson, S. Mattsson, G. Pédehontaa-Hiaa, C. Rääf, K. Sundin, L. Waldner, Assessment of "Zero Point" radiation around the ESS facility, Tech. Rep. MA RADFYS 2018:01, Lund University, 2018.

[27] P. Ström, D. Primetzhofer, Ion beam tools for nondestructive in-situ and in-operando composition analysis and modification of materials at the Tandem Laboratory in Uppsala, J. Instrum. 17 (04) (2022) P04011, http://dx.doi.org/10.1088/1748-0221/17/04/P04011.

[28] K. Arstila, J. Julin, M.I. Laitinen, J. Aalto, T. Konu, S. Kärkkäinen, S. Rahkonen, M. Raunio, J. Itkonen, J.-P. Santanen, T. Tuovinen, T. Sajavaara, Potku – New analysis software for heavy ion elastic recoil detection analysis, Nucl. Instrum. Methods Phys. Res. B 331 (2014) 34–41, http://dx.doi.org/10.1016/j.nimb.2014.02.016.

[29] V. Solé, E. Papillon, M. Cotte, P. Walter, J. Susini, A multiplatform code for the analysis of energy-dispersive X-ray fluorescence spectra, Spectrochim. Acta B: At. Spectrosc. 62 (1) (2007) 63–68, http://dx.doi.org/10.1016/j.sab.2006.12.002.

[30] G. Nagy, H.J. Whitlow, D. Primetzhofer, The scanning light ion microprobe in Uppsala – Status in 2022, Nucl. Instrum. Methods Phys. Res. B 533 (2022) 66–69, http://dx.doi.org/10.1016/j.nimb.2022.10.017.

[31] C.G. Ryan, D.R. Cousens, S.H. Sie, W.L. Griffin, G.F. Suter, E. Clayton, Quantitative pixe microanalysis of geological matemal using the CSIRO proton microprobe, Nucl. Instrum. Methods Phys. Res. B 47 (1) (1990) 55–71, http://dx.doi.org/10.1016/0168-583X(90)90047-X.

[32] C.G. Ryan, J.S. Laird, L.A. Fisher, R. Kirkham, G.F. Moorhead, Improved dynamic analysis method for quantitative PIXE and SXRF element imaging of complex materials, Nucl. Instrum. Methods Phys. Res. B 363 (2015) 42–47, http://dx.doi.org/10.1016/j.nimb.2015.08.021.

[33] R. Salminen, M.J. Batista, M. Bidovec, A. Demetriades, B. De Vivo, W. De Vos, m. Duris, A. Gilucis, V. Gregorauskiene, J. Halamic, P. Heitzmann, A. Lima, G. Jordan, G. Klaver, P. Klein, J. Lis, J. Locutura, K. Marsina, A. Mazreku, P.J. O'Connor, S.Å. Olsson, R.-T. Ottesen, V. Petersell, J. Plant, S. Reeder, I. Salpeteur, H. Sandström, U. Siewers, A. Steenfelt, T. Tarvainen, Geochemical atlas of Europe. Part 1 - Background information, methodology and maps, 2005.

[34] L.Y. Wang, M.S. Lee, A review on the aqueous chemistry of Zr(IV) and Hf(IV) and their separation by solvent extraction, J. Ind. Eng. Chem. 39 (2016) 1–9, http://dx.doi.org/10.1016/j.jiec.2016.06.004.

[35] Y.X. Liu, Q.X. Li, N. Ma, X.L. Sun, J.F. Bai, Q. Zhang, Application of the Zr/Hf ratio in the determination of Hafnium in geochemical samples by high-resolution inductively coupled plasma mass spectrometry, Anal. Chem. 86 (23) (2014) 11570–11577, http://dx.doi.org/10.1021/ac503517f.

[36] P. Pongrac, I. Kreft, K. Vogel-Mikus, M. Regvar, M. Germ, P. Vavpetic, N. Grlj, L. Jeromel, D. Eichert, B. Budic, P. Pelicon, Relevance for food sciences of quantitative spatially resolved element profile investigations in wheat (Triticum aestivum) grain, J. R. Soc. Interface 10 (84) (2013) 20130296, http://dx.doi.org/10.1098/rsif.2013.0296.

[37] J.L. Slavin, D. Jacobs, L. Marquart, Grain processing and nutrition, Crit. Rev. Food Sci. Nutr. 40 (4) (2000) 309–326, http://dx.doi.org/10.1080/10408690091189176.

[38] J. Pallon, V. Auzelyte, M. Elfman, M. Garmer, P. Kristiansson, K. Malmqvist, C. Nilsson, A. Shariff, M. Wegdén, An off-axis STIM procedure for precise mass determination and imaging, Nucl. Instrum. Methods Phys. Res. B 219–220 (2004) 988–993, http://dx.doi.org/10.1016/j.nimb.2004.01.201.

[39] L. Lyubenova, P. Pongrac, K. Vogel-Mikuš, G.K. Mezek, P. Vavpetič, N. Grlj, P. Kump, M. Nečemer, M. Regvar, P. Pelicon, P. Schröder, Localization and quantification of Pb and nutrients in Typha latifolia by micro-PIXE, Metallomics 4 (2012) 333–341, http://dx.doi.org/10.1039/C2MT00179A.

[40] H.J. Whitlow, A. Kuznetsov, A. Azarov, G. Nagy, R.J.W. Frost, N. Henderson, R. Greco, N. Deoli, K.M. Smith, W. Sudprasert, S. Amphalop, W. Insuan, S. Wichianchot, M.-Q. Ren, T. Osipowicz, C.G. Ryan, F. Villinger, Dynamic analysis of major elements in biological tissue validating trace element quantification of the trace life elements in MeV ion beam microscopy, Nucl. Instrum. Methods Phys. Res. B 554 (2024) 165411, http://dx.doi.org/10.1016/j.nimb.2024.165411.

[41] H.J. Whitlow, G. Nagy, A. Kuznetsov, R.J.W. Frost, A. Azarov, K.M. Smith, S. Amphalop, W. Insuan, S. Wichianchot, M.-Q. Ren, T. Osipowicz, C.G. Ryan, W. Sudprasert, F. Villinger, Major and trace element composition differences revealed in porcine intestine by dynamic analysis and mev ion microscopy, Physica Status Solidi (a) (2024) 2400161, http://dx.doi.org/10.1002/pssa.202400161.